AEDC-TR-86-6

Improvements in Code TUNCOR for Calculating Wall Interference Corrections in the Transonic Regime

M. H. Rizk
Flow Industries, Inc.
21414-68th Avenue South
Kent, Washington 98032

March 1986

Final Report for Period April 1983 – December 1985

ARNOLD ENGINEERING DEVELOPMENT CENTER
ARNOLD AIR FORCE STATION, TENNESSEE
AIR FORCE SYSTEMS COMMAND
UNITED STATES AIR FORCE

NOTICES

When U. S. Government drawings, specifications, or other data are used for any purpose other than a definitely related Government procurement operation, the Government thereby incurs no responsibility nor any obligation whatsoever, and the fact that the government may have formulated, furnished, or in any way supplied the said drawings, specifications, or other data, is not to be regarded by implication or otherwise, or in any manner licensing the holder or any other person or corporation, or conveying any rights or permission to manufacture, use, or sell any patented invention that may in any way be related thereto.

Qualified users may obtain copies of this report from the Defense Technical Information Center.

References to named commercial products in this report are not to be considered in any sense as an endorsement of the product by the United States Air Force or the Government.

This report has been reviewed by the Office of Public Affairs (PA) and is releasable to the National Technical Information Service (NTIS). At NTIS, it will be available to the general public, including foreign nations.

APPROVAL STATEMENT

This report has been reviewed and approved.

Keith L Kushman

KEITH L. KUSHMAN
Directorate of Technology
Deputy for Operations

Approved for publication:

FOR THE COMMANDER

Lowell C Keel

LOWELL C. KEEL, Lt Colonel, USAF
Director of Technology
Deputy for Operations

UNCLASSIFIED
SECURITY CLASSIFICATION OF THIS PAGE

REPORT DOCUMENTATION PAGE

1a REPORT SECURITY CLASSIFICATION UNCLASSIFED	1b RESTRICTIVE MARKINGS
2a SECURITY CLASSIFICATION AUTHORITY	3. DISTRIBUTION/AVAILABILITY OF REPORT Approved for public release; distribution unlimited.
2b DECLASSIFICATION/DOWNGRADING SCHEDULE	
4 PERFORMING ORGANIZATION REPORT NUMBER(S) AEDC-TR-86-6	5. MONITORING ORGANIZATION REPORT NUMBER(S)
6a NAME OF PERFORMING ORGANIZATION Flow Industries, Inc. 6b. OFFICE SYMBOL (If applicable)	7a NAME OF MONITORING ORGANIZATION
6c. ADDRESS (City, State and ZIP Code) 21414 68th Avenue South Kent, Washington 98032	7b ADDRESS (City, State and ZIP Code)
8a. NAME OF FUNDING/SPONSORING ORGANIZATION Arnold Engineering Development Center 8b. OFFICE SYMBOL (If applicable) DOT	9. PROCUREMENT INSTRUMENT IDENTIFICATION NUMBER F40600-83-C-0003
8c. ADDRESS (City, State and ZIP Code) Air Force Systems Command Arnold Air Force Station, TN 37389	10 SOURCE OF FUNDING NOS PROGRAM ELEMENT NO: 65807F PROJECT NO TASK NO WORK UNIT NO
11 TITLE (Include Security Classification) Please see reverse of this page.	
12 PERSONAL AUTHOR(S) Rizk, M.H., Flow Industries, Inc., Kent, Washington	
13a TYPE OF REPORT Final 13b. TIME COVERED FROM 4/83 TO 12/85	14 DATE OF REPORT (Yr., Mo., Day) March 1986 15 PAGE COUNT 35
16. SUPPLEMENTARY NOTATION Available in Defense Technical Information Center (DTIC).	

17. COSATI CODES		
FIELD	GROUP	SUB GR
20	04	

18 SUBJECT TERMS (Continue on reverse if necessary and identify by block number)
wind tunnel corrections transonic flow
wall interference

19. ABSTRACT (Continue on reverse if necessary and identify by block number)

Modifications are introduced to Code TUNCOR to allow its use in determining wall interference corrections in the AEDC 1T tunnel. The modifications include conversion to cylindrical coordinates and converting the measured pressure data to a form acceptable by the code.

20 DISTRIBUTION/AVAILABILITY OF ABSTRACT UNCLASSIFIED/UNLIMITED ☐ SAME AS RPT ☒ DTIC USERS ☐	21 ABSTRACT SECURITY CLASSIFICATION Unclassified
22a. NAME OF RESPONSIBLE INDIVIDUAL W.O. Cole	22b TELEPHONE NUMBER (Include Area Code) (615) 454-7813 22c OFFICE SYMBOL DOS

DD FORM 1473, 83 APR EDITION OF 1 JAN 73 IS OBSOLETE

UNCLASSIFIED
SECURITY CLASSIFICATION OF THIS PAGE

11. TITLE. Concluded.

Improvements in Code TUNCOR for Calculating Wall Interference Corrections in the Transonic Regime

PREFACE

The work reported herein was conducted by Flow Industries, Inc., 21414 - 68th Avenue South, Kent, Washington, under Air Force Contract F40600-83-C-0003 with Arnold Engineering Development Center/PK, Air Force Systems Command, Arnold Air Force Station, Tennessee. The AEDC Project Manager for this work was Dr. Keith L. Kushman, AEDC/DOT.

The reproducibles used in the reproduction of this report were supplied by the author.

CONTENTS

ILLUSTRATIONS

Figure

APPENDIX

NOMENCLATURE

1.0 INTRODUCTION

Wall interference effects are a limiting factor on the accuracy of data obtained from transonic wind tunnel tests. Classical linear theory[1] and modifications to this theory[2-5] provide an insight into the nature of these errors. However, sufficiently accurate estimates for practical use are not obtainable from linear theory. Kemp[6,7] formulated a procedure that uses nonlinear transonic computer codes to determine Mach number and angle-of-attack corrections. Murman[8] made improvements in Kemp's formulation and conducted a series of two-dimensional airfoil simulations to show that wall interference corrections are possible for strongly supercritical flows. Rizk and Murman[9] extended the approach of Kemp to practical three-dimensional geometries. They developed a computer code, TUNCOR, which estimates wind tunnel wall interference corrections. The purpose of this report is to describe modifications to code TUNCOR that increase its accuracy and allow it to be compatible with the AEDC 1T wind tunnel measurement system geometry.

In addition to Mach number and angle-of-attack corrections, the transonic correction procedure used in code TUNCOR provides an estimate of the accuracy of the corrections. Lift, pitching moment and pressure measurements near the tunnel walls are required. The correction procedure may be divided into two steps. In the first step, the flow about the test model is simulated numerically using the pressure measurements near the tunnel walls as boundary conditions. An inviscid transonic flow code is used for this purpose. In this step the wing and tail angles of attack, $\alpha_{T,w}$ and $\alpha_{T,t}$, are determined such that the calculated lift and pitching moment of the simulated model are equal to the measured lift and pitching moment, respectively. The angles of attack $\alpha_{T,w}$ and $\alpha_{T,t}$ will generally be different from the experimental values $\alpha_{e,w}$ and $\alpha_{e,t}$. This is due to the viscous effects present in the experiment but not in the numerical simulation of the flow and to geometrical differences between the test model and the simulated model. In the second step, the flow about the model in free air is numerically simulated. Angle-of-attack corrections and a free-stream Mach number correction are determined such that the calculated model lift and pitching moment match the experimental values and the calculated Mach number difference on the model surface in the tunnel and free air is minimized.

A summary of the correction procedure is given in Figure 1. A detailed description of the procedure is given in Ref. 9.

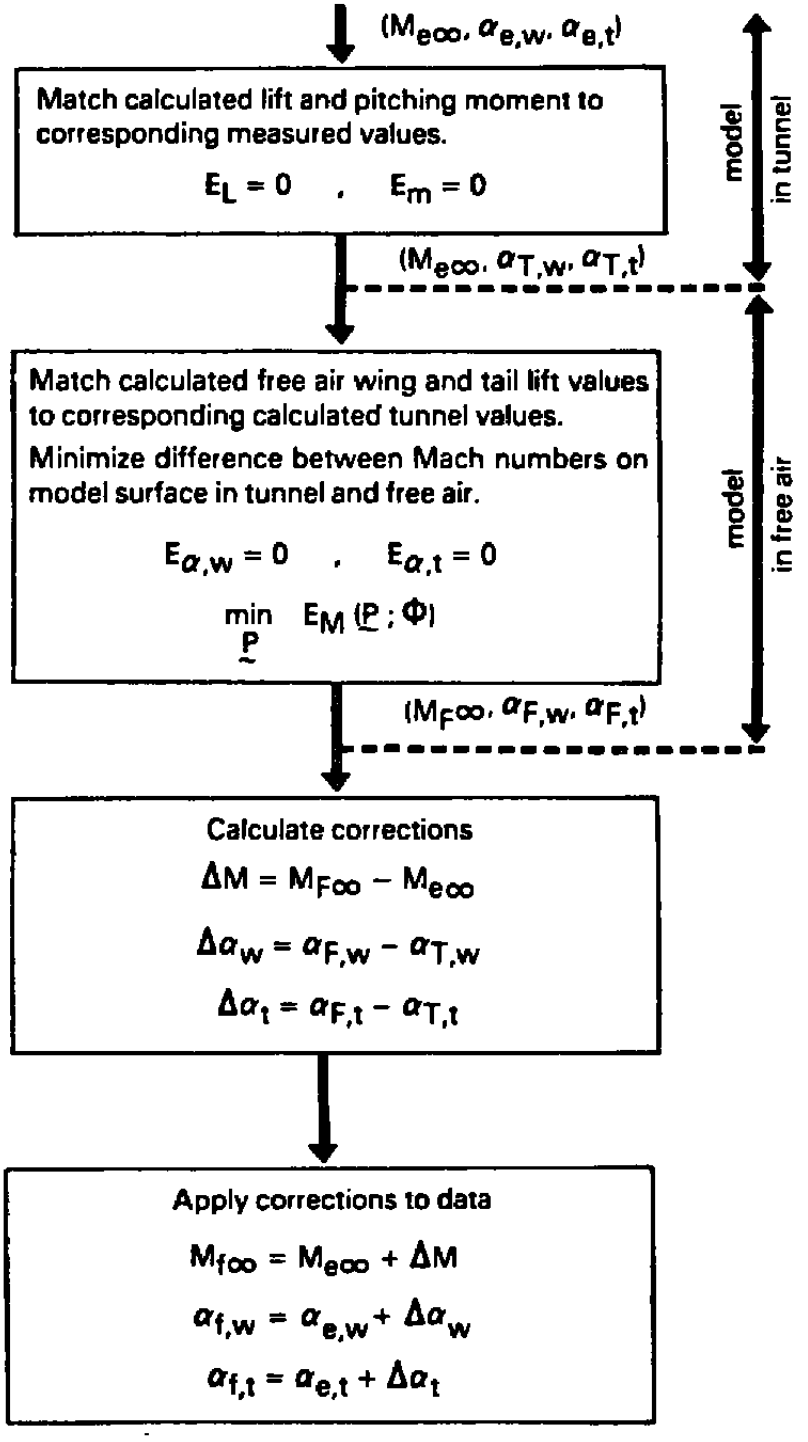

Figure 1. Correction procedure

2.0 SUMMARY OF MODIFICATIONS TO CODE TUNCOR

The correction procedure requires the numerical simulation of the flow about the test model. In code TUNCOR this simulation is achieved through the numerical solution of the transonic small disturbance equation. The formulation upon which the code is based assumes that pressure measurements are made on the boundaries of a rectangular parallelepiped with sides close to the tunnel walls but outside the boundary layer region (see Figure 2). In the first step of the correction procedure, the transonic small disturbance equation is therefore solved subject to the boundary conditions applied on the boundaries of the rectangular parallelepiped. A Cartesian coordinate system is used.

In the AEDC 1T tunnel, pressure measurements are made on a cylindrical surface (see Figure 3). Conversion to cylindrical coordinates is therefore necessary to allow proper numerical simulation of the tunnel flow subject to the measured boundary conditions.

Code TUNCOR calculates the flow in the tunnel subject to Dirichlet boundary conditions for the perturbation velocity potential ϕ on the side boundaries. It is therefore necessary to convert the measured data into boundary conditions that are acceptable by the code. Interpolation routines are also added so that boundary conditions at the computational mesh boundary points may be calculated.

Finally, improved accuracy is obtained by replacing the transonic small disturbance governing equation and the first-order boundary conditions by the full potential equation and second-order boundary conditions, respectively. A detailed description of the governing equation and boundary conditions is given in the following section.

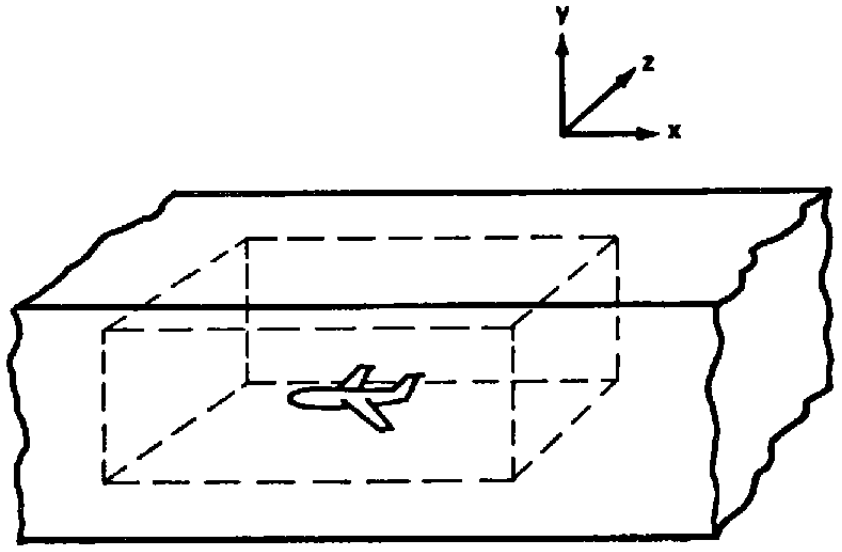

Figure 2. Geometrical configuration used in the original TUNCOR code

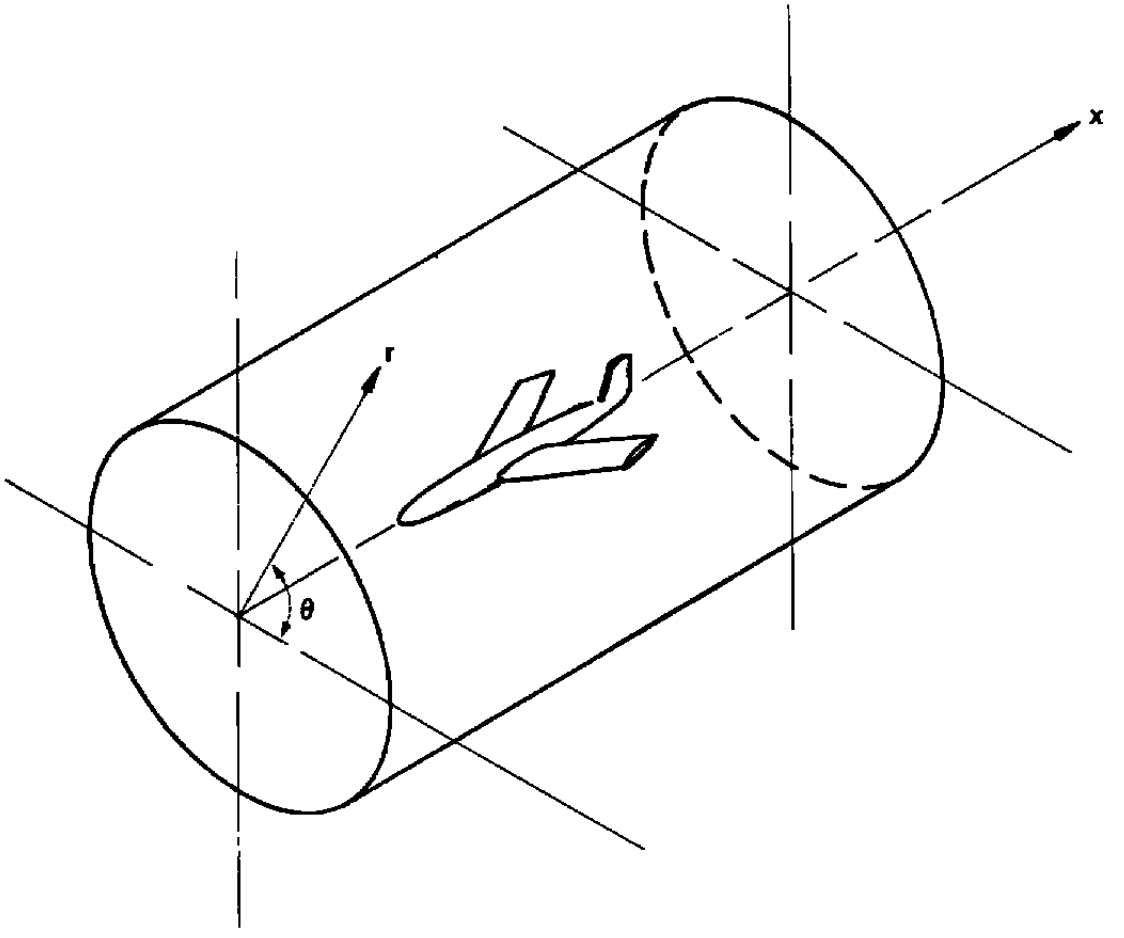

Figure 3. Cylindrical surface on which pressure measurements are made

3.0 GOVERNING EQUATIONS

3.1 FLOW GOVERNING EQUATION

The flow is governed by the continuity equation

$$\nabla\cdot(\rho\underline{q}) = 0$$

or

$$\frac{\partial}{\partial X}(\rho UR) + \frac{\partial}{\partial Y}(\rho v) + \frac{\partial}{\partial Z}(\rho wR) = 0 \tag{1}$$

where the velocity $\underline{q}$ is expressed in terms of the perturbation velocity potential function ϕ as follows:

$$\underline{q} = \nabla(X+\phi)$$

and the density ρ for an isentropic flow is given by

$$\rho = \left[1 + \frac{\gamma-1}{2} M_\infty^2 (1 - \underline{q}\cdot\underline{q})\right]^{\frac{1}{\gamma-1}} \tag{2}$$

The small disturbance assumption made in Ref. 9 allows expression (2) for ρ to be expanded in terms of a truncated binomial expansion. When this expansion is substituted into Eq. (1), the transonic small disturbance equation results. The full expression for ρ given by Eq. (2) is used in the present work.

3.2 MODEL BOUNDARY CONDITIONS

For a general body with a surface defined by

$$B(X,Y,Z) = 0$$

the boundary condition specifying zero flow through the body surface is given by

$$\underline{q}\cdot\nabla B = 0$$

This boundary condition may be expressed as

$$v = UR\frac{\partial Y_s}{\partial X} + wR\frac{\partial Y_s}{\partial Z} \qquad \text{on } Y = Y_s(X,Z) \tag{3}$$

and

$$w = U \frac{\partial Z_s}{\partial X} + \frac{v}{R} \frac{\partial Z_s}{\partial Y} \qquad \text{on } Z = Z_s(X,Y) \tag{4}$$

where the surfaces

$$Y = Y_s(X,Z) \text{ and } Z = Z_s(X,Y)$$

specify solid boundaries.

It is convenient to apply boundary conditions on coordinate surfaces when the problem is solved numerically. For surfaces that deviate slightly from the coordinate surface

$$Y = Y_o$$

it is possible to make the following Taylor series expansion:

$$(\rho v)\Big|_{Y = Y_o} = (\rho v)\Big|_{Y = Y_s} - (Y_s - Y_o) \frac{\partial(\rho v)}{\partial Y}\Big|_{Y = Y_s} + O\left[(Y_s - Y_o)^2\right] \tag{5}$$

Using Eq. (3) and Eq. (1) to express the first and second terms, respectively, on the right-hand side of Eq. (5), one gets

$$(\rho v)\Big|_{Y = Y_o} = \frac{\partial}{\partial X}\left[(\rho U R)(Y_s - Y_o)\right]\Big|_{Y = Y_s} + \frac{\partial}{\partial Z}\left[(\rho w R)(Y_s - Y_o)\right]\Big|_{Y = Y_s} + O\left[(Y_s - Y_o)^2\right] \tag{6}$$

For surfaces that deviate slightly from the coordinate surface

$$Z = Z_o$$

it is possible to make the following Taylor series expansion:

$$(\rho w R)\Big|_{Z = Z_o} = (\rho w R)\Big|_{Z = Z_s} - (Z - Z_o) \frac{\partial(\rho w R)}{\partial Z}\Big|_{Z = Z_s} + O\left[(Z_s - Z_o)^2\right] \tag{7}$$

Using Eq. (4) and Eq. (1) to express the first and second terms, respectively, on the right-hand side of Eq. (7), one gets

$$(\rho wR)\Big|_{Z = Z_o} = \frac{\partial}{\partial X}\left[(\rho UR)\,(Z_s - Z_o)\right]\Big|_{Z = Z_s} + \frac{\partial}{\partial Y}\left[(\rho v)\,(Z_s - Z_o)\right]\Big|_{Z = Z_s} + O\left[(Z_s - Z_o)^2\right] \tag{8}$$

The usual assumption that variations in the Z or Y directions are negligible relative to variations in the X direction is made here. It is therefore assumed that Y and Z derivatives on the right-hand sides of Eqs. (6) and (8) are $O[(Y_s - Y_o)^2]$ and $O[(Z_s - Z_o)^2]$, respectively. The boundary conditions are therefore

$$(\rho v)\Big|_{Y = Y_o} = \frac{\partial}{\partial X}\left[(\rho UR)\,(Y_s - Y_o)\right]\Big|_{Y = Y_s} + O\left[(Y_s - Y_o)^2\right] \tag{9}$$

$$(\rho wR)\Big|_{Z = Z_o} = \frac{\partial}{\partial X}\left[(\rho UR)\,(Z_s - Z_o)\right]\Big|_{Z = Z_s} + O\left[(Z_s - Z_o)^2\right] \tag{10}$$

The usual small disturbance boundary conditions are derived by making the following Taylor series expansions:

$$v\Big|_{Y = Y_o} = v\Big|_{Y = Y_s} + O(Y_s - Y_o)$$

$$(wR)\Big|_{Z = Z_o} = (wR)\Big|_{Z = Z_s} + O(Z_s - Z_o)$$

and then substituting expressions (3) and (4) for v and w into the above expansions after setting U = 1 and neglecting the last term on the right-hand side of Eqs. (3) and (4). Therefore,

$$v\Big|_{Y = Y_o} = R\,\frac{\partial Y_s}{\partial X} + O(Y_s - Y_o) \tag{11}$$

and

$$(wR)\Big|_{Z = Z_o} = \left(R\,\frac{\partial Z_s}{\partial X}\right)\Big|_{Z = Z_s} + O(Z_s - Z_o) \tag{12}$$

Boundary conditions (11) and (12) have been used in Ref. 9; however, the more accurate conditions (9) and (10) are used in this work.

In Ref. 9, a Cartesian computational mesh is used in the calculations. The small disturbance boundary conditions for the wing and tail are applied on planar mean surfaces in the usual manner. The body boundary conditions are also applied on the planar surfaces of a rectangular parallelepiped (see Figure 4). The boundary conditions at these surfaces are given by

$$\frac{\partial \phi^P(x,\theta)}{\partial N} = \frac{\partial \phi^b(x,\theta)}{\partial n} \frac{\partial S^b(x,\theta)/\partial \theta}{\partial S^P(\theta)/\partial \theta} \tag{13}$$

where $S^b(x,\theta)$ is the path length along the body cross-sectional contour at a given x station, $S^P(\theta)$ is the corresponding path length along the parallelepiped cross-sectional contour, n is the coordinate in the direction normal to the body contour, and N is the coordinate normal to the parallelepiped contour (see Figure 5). Relation (13) between the boundary condition applied on the rectangular parallelepiped and that applied on the body surface is chosen to match the mass flux introduced by the two conditions. Let the body cross-sectional contour at station x be defined by

$$r = r^b(x,\theta)$$

The value of $\partial S^b(x,\theta)/\partial\theta$ can then be expressed as

$$\frac{\partial S^b(x,\theta)}{\partial \theta} = \frac{r^b}{\cos \nu^b}$$

where

$$\nu^b = \frac{\pi}{2} - \tau^b$$

and τ^b is the angle between the body contour and the radial direction as indicated in Figure 5. Similarly, if the parallelepiped cross-sectional contour is defined by

$$r = r^P(\theta)$$

then the value of $\partial S^P(\theta)/\partial\theta$ is expressed as

$$\frac{\partial S^P(\theta)}{\partial \theta} = \frac{r^P}{\cos \nu^P}$$

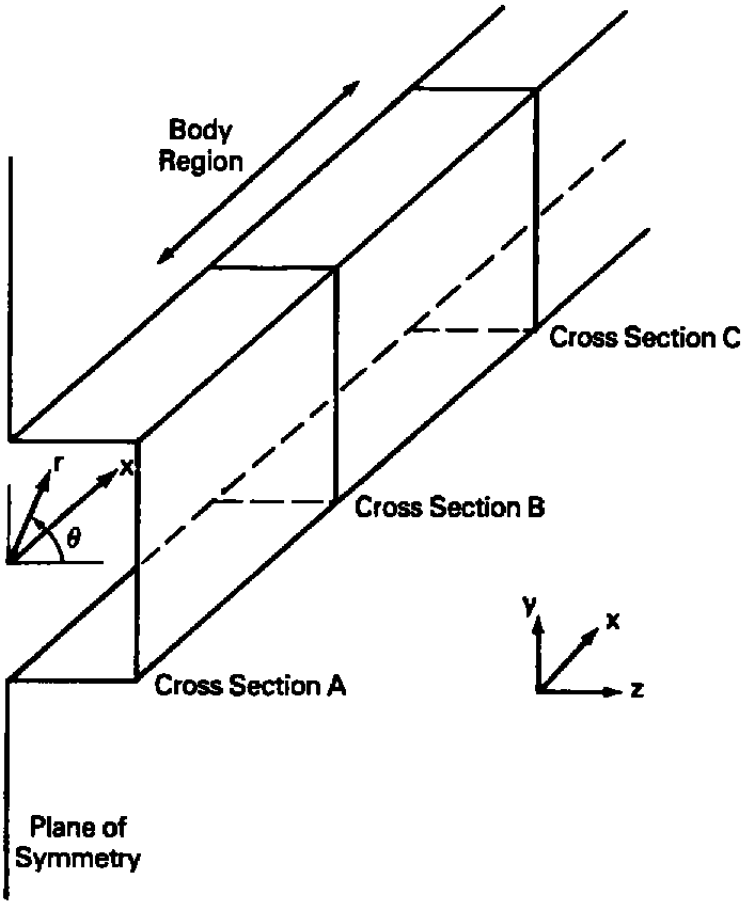

Figure 4. Parallelopiped on which body boundary conditions are applied

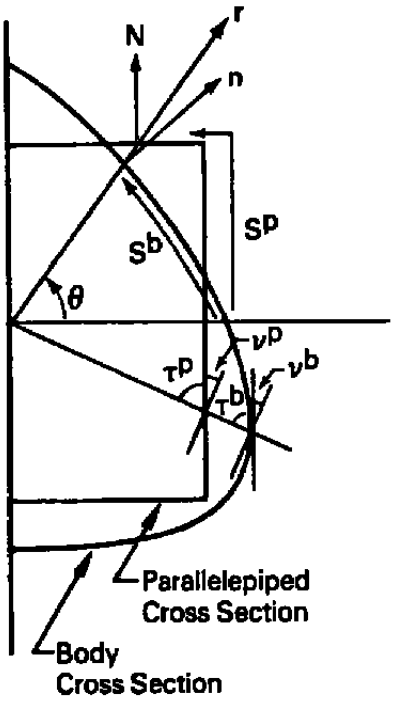

Figure 5. Body and parallelopiped cross-sectional contours

where

$$\nu^P = \frac{\pi}{2} - \tau^P$$

and τ^P is the angle between the parallelepiped contour and the radial direction as indicated in Figure 5. Boundary condition (13) applied at the parallelepiped surface may then be rewritten as

$$\frac{\partial\phi(x,\theta,r^P)}{\partial N} = \frac{\partial\phi(x,\theta,r^b)}{\partial n}\,\frac{r^b \cos \nu^P}{r^P \cos \nu^b} \tag{14}$$

As indicated in Figure 4, the rectangular parallelepiped extends over the length of the computational domain. Boundary condition (14) is valid, however, only in the interval along which the body extends (i.e., between Sections B and C). Beyond this interval, the right-hand side of Eq. (14) is replaced by zero.

The corresponding boundary condition formulation in cylindrical coordinates replaces the rectangular parallelepiped by a cylinder (see Figure 6). Eq. (14) is applied in the body region between Sections B and C. Here the boundary condition reduces to

$$\frac{\partial\phi(x,\theta,r_o)}{\partial r} = \frac{\partial\phi^b(x,\theta,r^b)}{\partial n}\,\frac{r^b}{r_o \cos \nu^b} \tag{15}$$

where r_o is the radius of the cylinder (see Figure 7). If the body is nearly axisymmetric, its cross-sectional contours will deviate only slightly from circular cross sections and, therefore, cos ν^b will be approximately equal to unity. In this case, cos ν^b may be replaced by 1 in Eq. (15). Upstream of Section B and downstream of Section C the condition

$$\frac{\partial\phi(x,\theta,r_o)}{\partial r} = 0$$

is applied.

The application of the body boundary conditions, in the manner described above, on a parallelepiped or a cylinder modifies the problem that was originally to be calculated. This formulation, however, does simplify the numerical calculations and is to be viewed as a crude approximation allowing the introduction of body effects into the problem without much complexity. Refinements that better approximate the original problem are possible and will be briefly described below. First, however, a description of the modified model that corresponds to the above formulation is given.

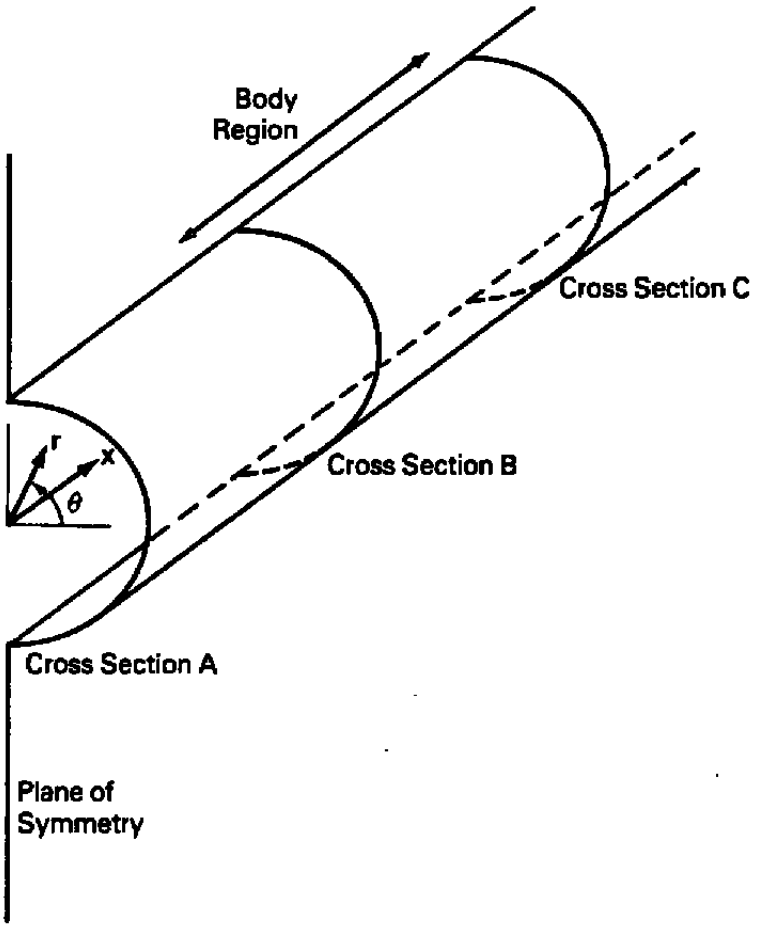

Figure 6. Cylinder on which body boundary conditions are applied

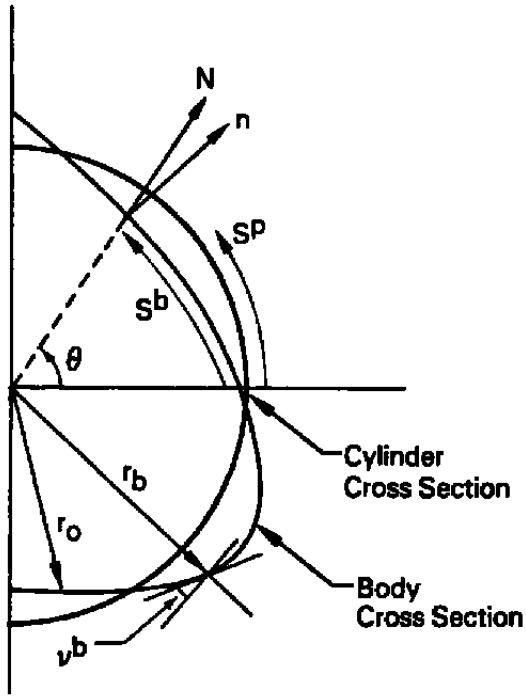

Figure 7. Body and cylinder cross-sectional contours

The application of the boundary condition

$$\frac{\partial\phi(x,\theta,r_o)}{\partial r} = 0$$

upstream of Section B and downstream of Section C corresponds to the introduction of a cylinder in these regions. Therefore, the flow cannot penetrate the surface of the cylinder. This is in contrast to the original problem in which the flow is not restricted upstream or downstream of the body. In the body region, between Sections B and C, the new formulation corresponds to a change in the original body shape. In the new formulation, the body becomes wrapped around the cylinder as indicated in Figure 8. This would indicate that as the cylinder radius reduces its effects in the body region and outside the body region also decrease.

Assuming that the body defined by

$$r = r_b(x,\theta)$$

is nearly axisymmetric, then the formulation that includes the cylinder of radius r_o will modify the boundary in the body region so that it is given by

$$r = r_s(x,\theta) = \sqrt{r_b^2(x,\theta) + r_o^2}$$

This formula indicates that, as r_o approaches 0, the modified body approaches the original body. Similarly, in the case of Cartesian coordinates, the modified body boundary is given by

$$y = y_s(x,\theta) = y_o + \left[\sqrt{r_b^2(x,\theta) + r_p^2(\theta)} - r_p(\theta)\right] \cos \nu^p$$

or

$$z = z_s(x,\theta) = z_o + \left[\sqrt{r_b^2(x,\theta) + r_p^2(\theta)} - r_p(\theta)\right] \cos \nu^p$$

Although not implemented in code TUNCOR, the following suggestions which give a better approximation to the original problem are briefly discussed here. In the case of Cartesian coordinates, the rectangular parallelepiped may be eliminated upstream of Section B and downstream of Section C. In this case, one will apply the body boundary conditions on the sides of the parallelepiped in the body region. This will better simulate the original body. Another suggestion is to eliminate the rectangular parallelepiped

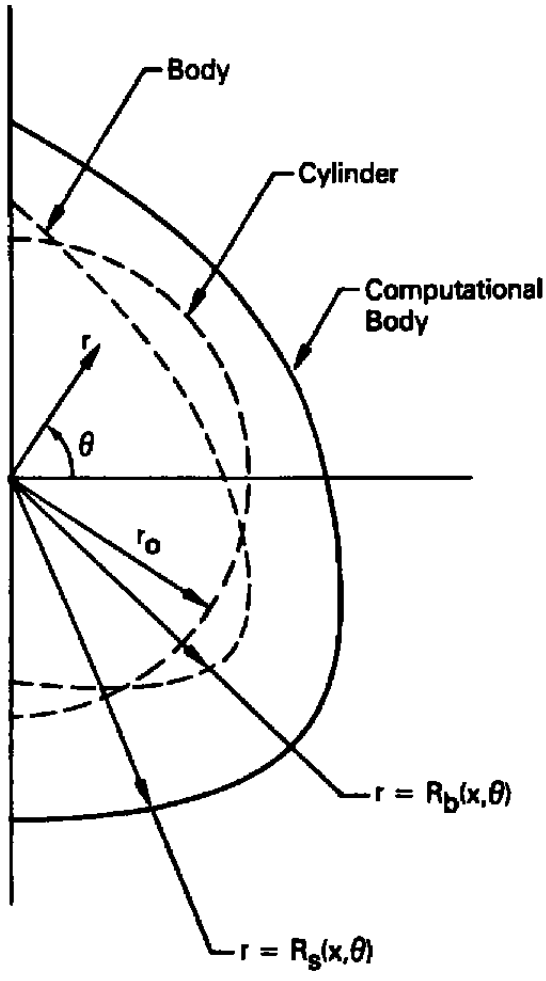

Figure 8. Cross section of computational body

upstream of Section B only. In this case, boundary conditions can be imposed downstream of Section C to model the wake region. The same suggestions apply to cylindrical coordinates; however, an additional complication occurs in this case. The governing equation in cylindrical coordinates is singular at the axis and, therefore, cannot be used to find the solution there. In this case, one may replace the cylinder outside the body region by a cylinder with a small diameter to reduce its effects there, or else one would be required to solve the governing equation on the axis in Cartesian coordinates while solving it elsewhere in cylindrical coordinates. The modifications suggested above will increase the accuracy of simulating the body; however, they would also increase the complexity of solving the equations.

4.0 FINITE DIFFERENCE EQUATIONS

The solution of the governing equation subject to the specified boundary conditions is found numerically. Therefore, a mesh of discrete points (X^i, Y^j, Z^k) with mesh spacings ΔX, ΔY, ΔZ is defined in the computational domain with

$$1 \leq i \leq I$$
$$1 \leq j \leq J$$
$$1 \leq k \leq K$$

All Neumann boundary conditions are applied on half-mesh coordinate surfaces (i.e., $Y = Y^{j+(1/2)}$ or $Z = Z^{k+(1/2)}$). We shall refer to mesh points neighboring boundary surfaces by boundary neighbor mesh points. Other mesh points away from boundaries are referred to as interior mesh points.

Discretizing Eq. (1) at the interior mesh point (i,j,k) leads to the following finite difference equation:

$$\left[(\rho UR)^{i+\frac{1}{2},j,k} - (\rho UR)^{i-\frac{1}{2},j,k}\right] \Big/ \Delta X + \left[(\rho v)^{i,j+\frac{1}{2},k} - (\rho v)^{i,j-\frac{1}{2},k}\right] \Big/ \Delta Y + \left[(\rho wR)^{i,j,k+\frac{1}{2}} - (\rho wR)^{i,j,k-\frac{1}{2}}\right] \Big/ \Delta Z = 0$$

This equation may be rewritten as

$$\frac{\partial^b}{\partial X}(\rho UR)^{i+\frac{1}{2},j,k} + \frac{\partial^b}{\partial Y}(\rho v)^{i,j+\frac{1}{2},k} + \frac{\partial^b}{\partial Z}(\rho wR)^{i,j,k+\frac{1}{2}} = 0 \qquad (16)$$

where $\frac{\partial^b}{\partial X}$, $\frac{\partial^b}{\partial Y}$, $\frac{\partial^b}{\partial Z}$ denote backward difference quotients.

The finite difference approximation to the governing equation at a mesh point (i,j,k) neighboring the computational boundary

$$Y = Y_o$$

is given by Eq. (16). However, now $(\rho v)^{i,j+(1/2),k}$ in this equation is replaced by the finite difference approximation to Eq. (9), where

$$Y_o = Y^{i,j,k} \pm \frac{1}{2} \Delta Y$$

Similarly, the finite difference approximation to the governing equation at a mesh point (i,j,k) neighboring the computational boundary

$$Z = Z_o$$

is given by Eq. (16). However, now $(\rho wR)^{i,j,k+(1/2)}$ in this equation is replaced by the finite difference approximation to Eq. (10), where

$$Z_o = Z^{i,j,k} \pm \frac{1}{2} \Delta Z$$

The finite difference approximation to the governing equation at a general mesh point (i,j,k) may be written as

$$\frac{\partial^b}{\partial X} \left[\rho UR(1 + \alpha_Y + \alpha_Z)\right]^{i+\frac{1}{2},j,k}$$

$$+ \frac{\partial^b}{\partial Y} (\rho v \, \beta_Y)^{i,j+\frac{1}{2},k} + \frac{\partial^b}{\partial Z} (\rho wR \, \beta_Z)^{i,j,k+\frac{1}{2}}$$

$$= 0 \qquad (17)$$

where the value of $\alpha_Y^{i+(1/2),j,k}$ is zero unless the mesh point $(X^{i+(1/2)}, Y^j, Z^k)$ neighbors the computational boundary

$$Y = Y_o$$

in which case

$$\alpha_Y^{i+\frac{1}{2},j,k} = \begin{cases} -\dfrac{Y_s - Y_o}{\Delta Y} & , \; Y^j = Y_o + \dfrac{1}{2} \Delta Y \\ \dfrac{Y_s - Y_o}{\Delta Y} & , \; Y^j = Y_o - \dfrac{1}{2} \Delta Y \end{cases}$$

or the mesh point $(X^{i+(1/2)}, Y^j, Z^k)$ neighbors the computational boundary

$$Z = Z_o$$

in which case

$$\alpha_Z^{i+\frac{1}{2},j,k} = \begin{cases} -\dfrac{R_s}{R}\ \dfrac{Z_s - Z_o}{\Delta Z} & , Z^k = Z_o + \dfrac{1}{2}\Delta Z \\ \dfrac{R_s}{R}\ \dfrac{Z_s - Z_o}{\Delta Z} & , Z^k = Z_o - \dfrac{1}{2}\Delta Z \end{cases}$$

The values of β_Y and β_Z are 1 except on computational boundaries normal to the Y and Z coordinates, respectively, where they are zero.

Finally, writing Eq. (17) in terms of the perturbation potential ϕ with

$$U = 1 + \phi_X$$
$$v = \frac{1}{R}\phi_Y$$
$$w = \phi_Z$$

and making the transformations

$$\xi = \xi(X)$$
$$\zeta = \zeta(Y)$$
$$\eta = \eta(Z)$$

with the objective of using a stretched mesh away from the aerodynamic model (at the model $\xi = X$, $\zeta = Y$, $\eta = Z$), the following is the resulting equation

$$\frac{\partial^b}{\partial\xi}\left[\frac{\tilde{R\rho}}{\zeta_Y\eta_Z}\left(1 + u_X\frac{\partial^c\phi}{\partial\xi}\right)(1 + a_Y + a_Z)\right]^{i+\frac{1}{2},j,k}$$
$$+\frac{\partial^b}{\partial\zeta}\left[\frac{\tilde{\rho}}{R\eta_Z\xi_X}\zeta_Y\phi\zeta\beta_Y\right]^{i,j+\frac{1}{2},k}$$
$$+\left[\frac{\partial^b}{\partial\eta}\frac{\tilde{R}\rho\eta_Z}{\xi_X\zeta_Y}\frac{\partial^c\phi}{\partial\eta}\beta_Z\right]^{i,j,k+\frac{1}{2}} = 0 \qquad (18)$$

where $\frac{\partial^c}{\partial\xi}$, $\frac{\partial^c}{\partial\eta}$, $\frac{\partial^c}{\partial\zeta}$ denote centered difference quotients and $\tilde{\rho}$ is the density modified by the artificial viscosity required for the stability of the difference scheme.

The above modifications have been introduced into computer code TUNCOR (see the appendix), which predicts Mach number and angle-of-attack corrections for wind tunnel models. The code has been submitted to AEDC where it is presently being tested.

REFERENCES

1. Garner, H.C., et al. "Subsonic Wind Tunnel Corrections." AGARDograph 109, October 1966.

2. Mokry, M., and Ohman, L.H. "Application of the Fast Fourier Transform to Two-Dimensional Wind Tunnel Wall Interference." J. Aircraft, Vol. 17, June 1980, pp. 402-408.

3. Mokry, M. "Subsonic Wall Interference Corrections for Finite Length Test Sections Using Boundary Pressure Measurements." Paper 10, AGARD Fluid Dynamics Panel Specialists' Meeting on Wall Interference in Wind Tunnels, May 1982.

4. Rizk, M.H., and Smithmeyer, M.G. "Wind-Tunnel Wall Interference Corrections for Three-Dimensional Flows." J. Aircraft, Vol. 19, June 1982, pp. 465-472.

5. Rizk, M.H. "Higher-Order Flow Angle Corrections for Three-Dimensional Wind Tunnel Wall Interference." J. Aircraft, Vol. 19, October 1982, pp. 893-895.

6. Kemp, W.B., Jr. "Toward the Correctable-Interference Transonic Wind Tunnel." AIAA 9th Aero Testing Conference, 1976, pp. 31-38.

7. Kemp, W.B., Jr. "Transonic Assessment of Two-Dimensional Wind Tunnel Wall Interference Using Measured Wall Pressures." NASA CP 2045, 1979.

8. Murman, E.M. "A Correction Method for Transonic Wind Tunnel Wall Interference." AIAA Paper 79-1533, July 1979.

9. Rizk, M.H., and Murman, E.M. "Wind Tunnel Wall Interference Corrections for Aircraft Models in the Transonic Regime." Report No. 244, Research and Technology Division, Flow Industries, Inc., Kent, WA, September 1982.

APPENDIX A
COMMENTS ABOUT COMPUTER CODE TUNCORC

Code TUNCOR (Ref. 9) has been developed to evaluate wind tunnel wall interference corrections for three-dimensional aircraft (wing-body-tail) configurations. The modified version of this code (TUNCORC) allows the option of using a cylindrical coordinate system in addition to the original Cartesian coordinate option. Also, code TUNCORC allows the use of the full potential equation with second-order boundary conditions in addition to the original option of using the small disturbance equation with first-order boundary conditions. Finally, code TUNCORC includes subroutines that transform the measured pressure data (on either a cylindrical surface or planar surfaces) to the corresponding potential function at the computational boundary for use in solving the tunnel boundary value problem. The code evaluates Mach number and angle-of-attack corrections by the theory developed in Ref. 9 and in the main text of this report. Code TUNCORC includes a user's manual. The comments given here are not intended to give a complete description of the code; however, they complement the user's manual included in code TUNCORC.

Code TUNCORC uses a simple Cartesian (or cylindrical) computational mesh. The mesh point coordinates are (X^i, Y^j, Z^k) where

$$i = 1, 2, \ldots, I$$
$$j = 1, 2, \ldots, J$$
$$k = 1, 2, \ldots, K$$

The computational mesh is uniform inside a rectangular parallelepiped (or cylinder) enclosing the model. Outside the parallelepiped (or cylinder), the mesh is stretched. The model surface boundary conditions are applied on half-mesh planar surfaces (i.e., $X = X^{i+(1/2)}$ or $Y = Y^{j+(1/2)}$ or $Z = Z^{k+(1/2)}$). This requires a number of modifications to the input geometrical model configuration. In other words, due to the simplicity of the computational mesh, the flow is generally computed about a modified model that differs slightly from the input model. A discussion of the nature of these modifications is given in this appendix.

The user has the freedom to specify the mesh spacings ΔY and ΔZ. The mesh spacing ΔX, however, cannot be arbitrarily specified if the sweep angle of the wing leading edge ψ_w is nonzero. The mesh spacing ΔX is restricted to

$$\Delta X = \frac{\Delta Z}{n} \tan \psi_w \quad , \quad n = 1, 2, \ldots$$

This restriction on ΔX allows the wing leading edge to pass through the mid-point between neighboring mesh points in the X direction as shown in Figure A-1. In the case of a leading-edge sweep angle of zero, the user may specify ΔX. Once ΔX is determined, the tail leading edge is restricted to one of the following sweep angles.

$$\psi_t' = \tan^{-1}\left(n \frac{\Delta X}{\Delta Z}\right), \quad n = 0, 1, 2, \ldots$$

Therefore, the code will adjust the input sweep angle θ_t to the closest allowable value ψ_t'. The tail is also displaced in the Z direction so that its base lies on the parallelepiped (or cylindrical) surface on which the body boundary condition is applied (see Figure A-1). This parallelepiped is specified by the user; however, the parallelepiped also is modified so that its planes lie at the mid-distance between two neighboring mesh planes.

As part of the output, the code prints any adjusted value and the corresponding input value.

The input data are shown below for the calculated example. In this example, all dimensions are evaluated in inches. The user, however, has the freedom of choosing the length units. Pressure measurements in the wind tunnel are given in the input data in terms of the corresponding pressure coefficients. The measured lift XLFTE and the measured moment XMOME are normalized by the total pressure, so that XLFTE and XMOME have the dimensions (unit length)^2 and (unit length)^3, respectively. The model lift normalized by the total pressure is given by

$$\frac{\hat{L}}{\hat{P}_o} = \int_{\substack{\text{model}\\ \text{surface}}} \frac{1}{\left(1 + \frac{\gamma-1}{2} M^2\right)^{\frac{\gamma}{\gamma-1}}} \, \underset{\sim}{n} \cdot \underset{\sim}{k} \, d\hat{S}$$

while the model lift normalized by $\hat{\rho}_\infty \hat{U}_\infty$ is given by

$$\frac{\hat{L}}{\hat{\rho}_\infty \hat{U}_\infty^2} = \frac{\left(1 + \frac{\gamma-1}{2} M_\infty^2\right)^{\frac{\gamma}{\gamma-1}}}{\gamma M_\infty^2} \int_{\substack{\text{model}\\ \text{surface}}} \frac{1}{\left(1 + \frac{\gamma-1}{2} M^2\right)^{\frac{\gamma}{\gamma-1}}} \, \underset{\sim}{n} \cdot \underset{\sim}{k} \, d\hat{S}$$

The first expression is used in the code since it is independent of free-stream conditions (M_∞).

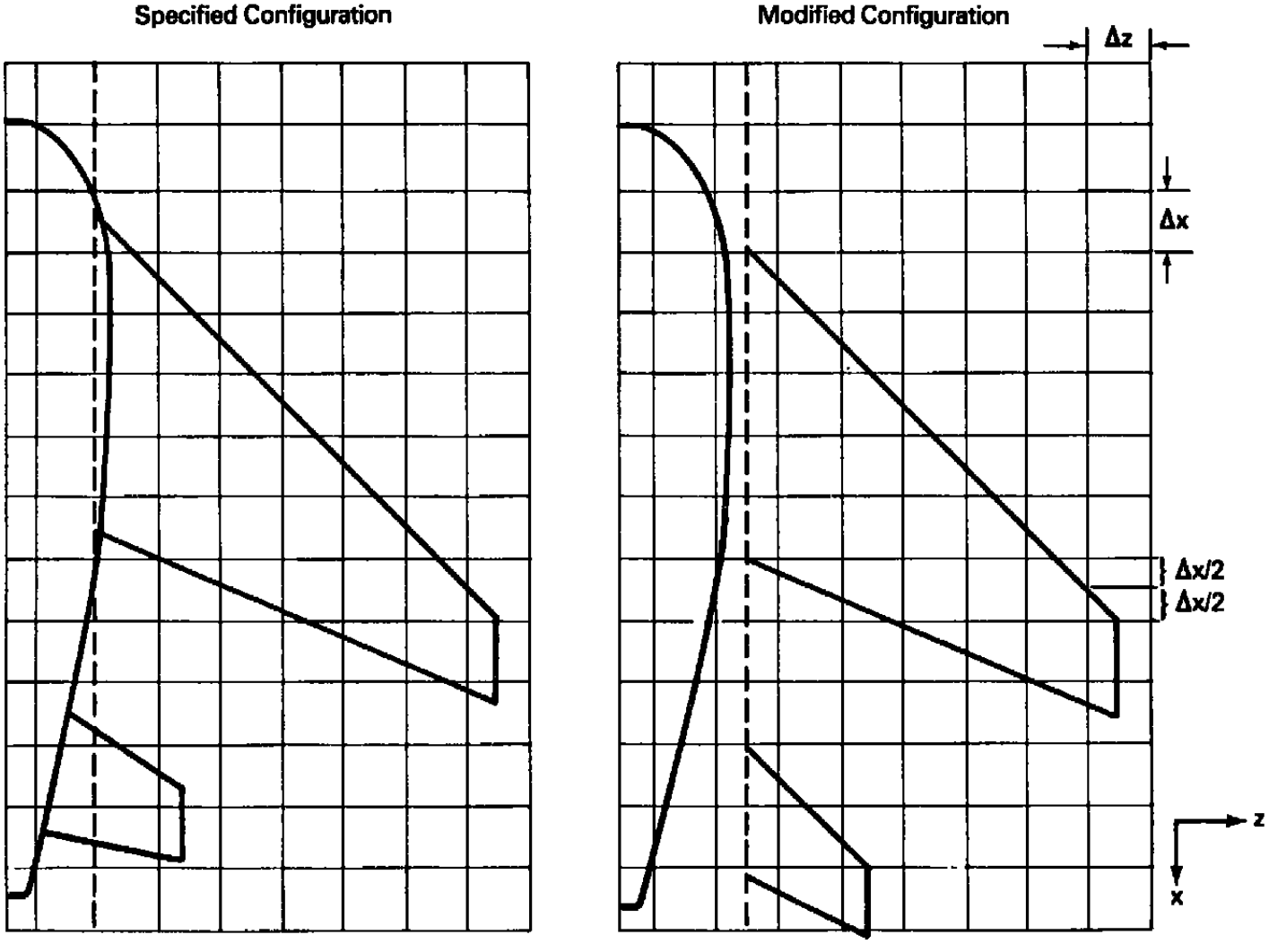

Figure A-1. Input and computed configurations

NOMENCLATURE

$E_L = \dfrac{L_{T,d}(\underset{\sim}{p};\phi) - L_{e,d}}{L_{e,d}}$

$E_m = \dfrac{m_{T,d}(\underset{\sim}{p};\phi) - m_{e,d}}{m_{e,d}}$

$E_M = \dfrac{\int (M_F - M_T)^2 \, ds}{\int M_T^2 \, ds}$

$E_{\alpha,t} = \dfrac{L_{F,t}(\underset{\sim}{P};\phi) - L_{T,t}(\underset{\sim}{p};\phi)}{L_{T,t}(\underset{\sim}{p};\phi)}$

$E_{\alpha,w} = \dfrac{L_{F,w}(\underset{\sim}{P};\phi) - L_{T,w}(\underset{\sim}{p};\phi)}{L_{T,w}(\underset{\sim}{p};\phi)}$

$\underset{\sim}{k}$ = unit vector vertically upward

L = lift/P_o

$\hat{L}$ = lift

m = pitching moment about the axis $x = x_m/P_o$

M = Mach number

$\underset{\sim}{n}$ = unit vector normal to model surface

$\underset{\sim}{p} = (\alpha_{T,w}, \alpha_{T,t})$

$\underset{\sim}{P} = (M_{F\infty}, \alpha_{F,w}, \alpha_{F,t})$

P_o = total pressure

q = velocity normalized by free-stream velocity magnitude

R = $\begin{cases} 1 & \text{, Cartesian coordinates} \\ r & \text{, cylindrical coordinates} \end{cases}$

u,v,w = perturbation velocity components normalized by free-stream velocity magnitude in X,Y,Z directions

U = $1 + u$

$\hat{U}$ = velocity component in the X direction

x,y,z = Cartesian coordinate system

x, θ, r = cylindrical coordinate system

x_m = x coordinate of axis about which the model pitching moment is measured

X = x

Y = y, Cartesian coordinates
    θ, cylindrical coordinates

Z = z, Cartesian coordinates
    r, cylindrical coordiates

α = angle of attack

γ = ratio of specific heats

ΔM = Mach number correction

$\Delta\alpha$ = angle-of-attack correction

ρ = density normalized by free-stream density

$\hat{\rho}$ = density

ϕ = perturbation velocity potential for the tunnel flow

Φ = perturbation velocity potential for the free-air flow

Subscripts

d = model

e = measured quantity or experimental condition

f = corrected condition

F = calculated quantity for the model in an inviscid free-air flow

M = Mach number

s = model surface

t = tail

T = calculated quantity for the model in an inviscid tunnel flow

w = wing

∞ = undisturbed condition